

1  
2  
3 **Regional Climate Model Simulation of Surface Moisture Flux Variations in Northern**  
4 **Terrestrial Regions**  
5

6 Ross Fischer<sup>1</sup>, John E. Walsh<sup>2</sup>, Eugénie S. Euskirchen<sup>3</sup>, and Peter A. Bieniek<sup>2</sup>

7 <sup>1</sup>University of Colorado, Boulder, CO

8 <sup>2</sup>International Arctic Research Center, University of Alaska, Fairbanks, AK

9 <sup>3</sup>Institute of Arctic Biology, University of Alaska, Fairbanks, AK  
10  
11  
12  
13  
14  
15  
16  
17  
18  
19

20 Corresponding author:

21 John Walsh

22 International Arctic Research Center

23 University of Alaska, Fairbanks, AK 99709

24 jwalsh@iarc.uaf.edu  
25

26 Submitted to the Journal of Hydrometeorology Atmospheric and Climate Sciences

27 September-December 2017

## ABSTRACT

The wetness of high-latitude land surfaces is strongly dependent on the difference between precipitation (P) and evapotranspiration (ET). If climate models are to capture the trajectory of surface wetness in high latitudes, they must capture the seasonality, the variations and the drivers of variations in the surface moisture fluxes. In this study, ~~a~~Variations of high-latitude ET over daily, seasonal, and interannual timescales are poorly documented, as are their relationships to key drivers such as precipitation and temperature, T. A combination of regional climate model output and eddy covariance measurements from flux tower locations in Alaska is used to evaluate model simulations of the surface moisture fluxes and their variations. In particular, we use the model output and the field measurements to test the ~~test the~~ hypothesis that temperature is the key driver of variations of ET in tundra regions underlain by permafrost, while precipitation plays a greater role in boreal forest areas. Although the model depicts a stronger hydrologic cycle (larger P, larger ET) relative to the *in situ* measurements at all the sites, the strong seasonal cycles of P, T, and ET are captured by the model. The tower measurements from all sites show a short period (one or two months) of negative P-ET during summer, indicative of surface drying, although the model does not show this period of drying in the tundra region in the foothills of the Brooks Range. At all the tundra sites, both the flux tower data and the model simulations show that daily and warm-season totals of ET are largely temperature-driven. Daily ET shows a weak negative correlation with precipitation ~~at in the measurements and in the model simulations of all the sites~~all the sites. Precipitation is the main driver of year-to-year variations of the seasonally integrated net moisture flux at all the sites, implying that precipitation will be at least as important as temperature in the future trajectory of surface wetness.

51  
52 *Keywords:* Evapotranspiration, precipitation, Arctic, tundra, boreal forest, moisture budget  
53  
54

## 55 **1. Introduction**

56 Some of the largest and most consequential uncertainties in the trajectory of the Arctic  
57 climate system are associated with the hydrology of the Arctic terrestrial surface. The challenge  
58 facing the research community is to provide a scientifically sound response to the fundamental  
59 question: Will Arctic landscapes become wetter or drier as climate changes? Because this  
60 question pertains to the future, model simulations must be relied upon for guidance. While there  
61 are important scaling issues ~~that are discussed below~~ associated with the validation and use of  
62 model output, in situ measurements of surface moisture flux measurements in recent decades  
63 now makes it possible to perform direct comparisons of measured and model-derived fluxes at a  
64 variety of high-latitude terrestrial sites.

65 ~~At the heart of the model validation issue is the ability of the model to capture the net~~  
66 ~~surface moisture flux, which is the difference between~~ major uncertainty surrounds the surface  
67 ~~moisture budget and the relationship between~~ precipitation (P) and evapotranspiration (ET). If P  
68 (including both rain and snow) exceeds ET over a period of time, the excess goes into runoff or  
69 storage. If ET exceeds P, the surface moisture deficit leads to drying unless there is sufficient  
70 recharge from below. A drying surface leads to decreased water supplies, increased wildfire  
71 risk, and moisture stress on vegetation, all of which have consequences for terrestrial ecosystems  
72 and human activities.

—In a recent synthesis of Arctic terrestrial hydrology, Bring et al. (2016, p. 642) conclude that “We are still lacking a comprehensive picture of evapotranspiration across Arctic regions and how it will interact with climate and landscape changes”. Arctic hydrology is constrained by permafrost in its northern subregions, and changes in permafrost as well as vegetation will undoubtedly affect the trajectory of Arctic terrestrial hydrology, particularly the wetness of the surface. This paper focuses on evapotranspiration, especially variations relative to precipitation and temperature (T), two of the key drivers of terrestrial hydrology.

The most comprehensive assessment of recent P and ET trends based on historical data and model simulations appears to be that of Rawlins et al. (2010), who used a variety of precipitation datasets, atmospheric reanalyses, land surface model output, and global climate models. Trends in P, ET, P-ET and river discharge were generally positive in the observational data, for which record lengths ranged from 20 to 50 years. However, trends of P-ET, computed as differences between historical P datasets and satellite-derived (AVHRR GIMMS) ET, showed no significant trend. The nine global climate models examined by Rawlins et al. (2010) showed statistically significant trends of *terrestrial* pan-Arctic P-ET over the period 1950-1999 in eight of the nine cases, and in all nine cases for the period 1950-2049. Trends for the historical period were smaller than for the future period in the climate model output. All results were for annual means. The positive trends in annual mean P-ET contrast with the expectation that longer and warmer summers will increase ET sufficiently to favor summer drying, which is indicated by projected decreases of high-latitude soil moisture in major climate change assessments such as the IPCC (2013, Figs. 11.14 and 12.23). Anticipated increases of high-latitude wildfire activity (Partain et al., 2016; Flannigan et al., 2015) are consistent with this expectation, highlighting the mixed picture of future surface wetness trends in the Arctic.

96 Laine et al.'s (2014) more recent evaluation of global climate model projections, although  
97 global rather than Arctic in scope, highlights the challenge of assessing changes in high-latitude  
98 surface wetness. While Laine et al. found that the projected changes of ET also show the  
99 expected pattern of increases over Arctic land areas, primarily during summer, the projected  
100 changes of P-ET over the Arctic were much less spatially coherent and less robust than the  
101 changes of P and ET separately. In particular, summer P-ET is projected to decrease over  
102 northern Canada, increase over Alaska, decrease over the western and northern Eurasian  
103 subarctic, and increase over parts of northeastern Russia, including Chukotka. Over most of these  
104 areas, the sign of the projected change was not robust across the models at the 95% confidence  
105 level. The spatial pattern over high-latitude land areas is very consistent with the projected  
106 changes in soil moisture obtained by Dirmeyer et al. (2014) using 15 of the same models.  
107 Dirmeyer et al.'s Figure 1 shows reductions of summer soil moisture over northern Canada and  
108 north-central Russia, but not over Alaska and eastern Siberia, from the preindustrial to the 20<sup>th</sup>  
109 century. The results of these studies highlight the uncertainty in the trajectory of surface wetness  
110 in Arctic land areas in the present generation of global climate models. Given this uncertainty  
111 and the reliance on models for anticipation of future changes in surface wetness, it is imperative  
112 to (1) understand the drivers of variations and changes in high-latitude ET, and (2) assess the  
113 ability of models to capture the relationship between the atmospheric drivers and variations of  
114 ET. The present paper addresses both of these needs.

115 The modeling studies highlighted above were based on global climate model simulations.  
116 There has been little evaluation of corresponding simulations by regional climate models, which  
117 offer several advantages relative to global climate models. First, regional climate models enable  
118 finer resolution, by up to an order of magnitude, relative to global climate models. Second, when

driven at the lateral boundaries by historical reanalyses, regional climate models are constrained to observations, at least at the lateral boundaries, while global models are freer to drift to their own model climatologies. For these reasons, the present study makes use of a regional climate model driven at the lateral boundaries by an atmospheric reanalysis.

A key measure of the validity of the ET simulations by climate models is their ability to capture the sensitivity of ET to variations of precipitation and temperature. During the growing season, ET can be expected to increase with temperature in biomes that are not moisture-limited (e.g., tundra underlain by permafrost). One might also expect ET to respond positively to precipitation events in areas where ET is moisture limited (e.g., permafrost-free boreal forest sites). The expectation of influences by temperature (T) and precipitation (P) is supported by variations in yearly ET, T, and P at tundra sites in Alaska (Euskirchen et al., 2012) and Canada (Lafleur and Humphreys, 2007). Other variables undoubtedly play a role in temporal variability of ET. For example, solar and longwave radiation are included in ET formulations (e.g., Penman-Monteith) and are important drivers of Arctic ecosystem production (e.g., Lafleur et al., 2012). Changes in subsurface moisture, including moisture made available by permafrost thaw, can also be an important driver (Ohta et al., 2008). However, because direct measurements of these quantities are greatly limited compared to T, P, and ET, the diagnostic evaluation in the present study focuses on P and T as key drivers. Against this backdrop of prior studies, hypotheses and data constraints, we address two key questions:

- 1) How well are the surface moisture fluxes, variations, and relationships to key drivers over timescales of days to seasons captured by a state-of-the-art regional climate model?

Formatted: Font: (Default) Times New Roman, 12 pt

Formatted: Numbered + Level: 1 + Numbering Style: 1, 2, 3, ... + Start at: 1 + Alignment: Left + Aligned at: 0.25" + Indent at: 0.5"

2) How strongly do temperature and precipitation influence variations of  
relationships between temperature, precipitation and surface moisture fluxes over daily to  
seasonal timescales? flux variations reproduced by the regional climate model?

2- Both these questions point to the paper's emphasis on model validation. Because inter-  
variable relationships are part of the validation in (2), an assessment of processes and drivers is  
implicitly part of our model evaluation strategy. In that respect, the following sections include  
discussion of the drivers and processes relevant to variations of the surface moisture budget. In  
all cases, however, the consistency (or lack thereof) between the simulated and observed  
relationships is the underlying thread of the discussion.

Formatted: Normal, Indent: First line: 0.31", No bullets or numbering

~~3- How well are the surface moisture fluxes, variations, and relationships to key drivers  
captured by a state-of-the-art climate model?~~

Formatted: Font: (Default) Times New Roman, 12 pt

—The study focuses on the tundra and boreal forest biomes of Alaska, where *in situ*  
measurements of the moisture fluxes and drivers are available for several sites in each biome. A  
regional climate model provides the simulated fluxes and driving variables for the same years  
and locations. In this study we refer to temperature and precipitation as “drivers” of ET and P-  
ET only in a proxy sense. In reality, ET is driven by radiative fluxes (for which temperature may  
be regarded as a proxy), boundary layer stability (which is also affected by surface air  
temperatures), relative humidity and vertical humidity gradients (which are affected by  
precipitation), and wind speed. Our emphasis on temperature and precipitation is dictated in part  
by the availability of these variables, especially from the nearby weather observing sites used for  
the infilling of missing values at the tower sites.

161 ~~Both of these sources of hydrologic information are described in Section 2~~  
162 ~~describes the two sources of hydrologic information: the regional climate model and the in situ~~  
163 ~~measurements. The Section 3 describes the processing of the model output and the in situ~~  
164 ~~measurements, including their quality-control is described in Section 3. Section 4~~  
165 ~~presents the results in terms of seasonal climatologies as well as interannual variations derived~~  
166 ~~from both sources. The relationships of ET and P-ET to the atmospheric drivers are evaluated in~~  
167 ~~Section 5 for seasonal and daily timescales. Discrepancies between the observational data and~~  
168 ~~the model results are highlighted in both Sections 4 and 5. Section 6 summarizes the primary~~  
169 ~~conclusions.~~

## 170 2. Sources of data

### 171 2.2.1. Regional climate model output

172 Global model output is available from several dozen climate modeling centers, and the  
173 hydrologic output from the current generation of these models (CMIP5, Coupled Model  
174 Intercomparison Project, version 5) has been evaluated by Rawlins et al. (2010), Laine et al.  
175 (2014) and Yao et al. (2016). For comparison with site-specific measurements such as those in  
176 Section 2.1, finer resolution of model output is highly desirable. Dynamical downscaling by a  
177 regional climate model can achieve finer resolution by approximately an order of magnitude. In  
178 this study, we analyze P, T, and ET from a widely used regional climate model, the Advanced  
179 Research (ARW) core of the Weather Research and Forecasting (WRF) model (Skamarock et al.  
180 2008). The model makes use of a thermodynamic sea ice model (Zhang and Zhang 2001) and  
181 the Noah land-surface model (Yang et al., 2011) used within WRF in order to model the thermal  
182 conditions at the surface. It is driven at the lateral boundaries by observationally-based

Formatted: Indent: Left: 0", Numbered + Level: 1 +  
Numbering Style: 1, 2, 3, ... + Start at: 2 + Alignment: Left +  
Aligned at: 0.25" + Indent at: 0.5"

Formatted: Font: (Default) Times New Roman, 12 pt, Italic

Formatted: Font: (Default) Times New Roman, 12 pt, Italic

Formatted: Normal, No bullets or numbering

Formatted: Font: (Default) Times New Roman, 12 pt



reanalysis fields (ERA-Interim) in order to avoid introduction of additional biases arising from the driving model. The ERA-Interim reanalysis was selected as it has been successfully downscaled using WRF in other regions of the world (e.g. Gao et al. 2015; Srivastava et al. 2014, 2013; Soares et al. 2012), has been used in previous Arctic WRF simulations and analyses (e.g. Liu et al. 2014) and is among the best performing reanalysis data sets for Alaska (Lader et al. 2015) and the wider Arctic (Lindsay et al. 2014).

As described by Bieniek et al. (2016), the downscaling covered a domain with 262x262 grid points that encompassed all of Alaska and portions of far eastern Russia and northern Canada at 20 km horizontal resolution (Figure 41) with 49 vertical model levels. The model was reinitialized every two days and was integrated for a total of 54 hours after each reinitialization. Each initialization occurred at 18 UTC (09 AKST). After each reinitialization, the first 6 hours of output (a “spin-up” overlapping with the final 6 hours of the previous 54-hour integration) were discarded. The frequent reinitialization to the ERA-Interim reanalysis, together with a continuous nudging to the ERA-Interim upper air fields during each 54-hour simulation, ensured that the model was tightly constrained by the observationally-based reanalysis.

The output from the 2-day simulations was combined together to form the final downscaled product, which spanned the 1979-2015 period. Hourly WRF output was saved and used to produce daily mean values of downscaled variables. The daily ET values were calculated from the daily values of latent heat flux in the archive of model output. (The same conversion was performed with the *eddy covariance in situ* measurements described below). The daily mean values of T, P, and ET from the model’s 20-km grid cells corresponding to the tower sites of Section 2.1 were extracted for the years of the available tower data (Section 3)-validation data.

Formatted: Font: (Default) Times New Roman, 12 pt

Formatted: Font: (Default) Times New Roman, 12 pt

Formatted: Font: (Default) Times New Roman, 12 pt

Formatted: Font: Italic

Formatted: Font: (Default) Times New Roman, 12 pt

Formatted: Font: (Default) Times New Roman, 12 pt

Formatted: Font: (Default) Times New Roman, 12 pt

4-

## 2.12.2 *In situ measurements*

Eddy covariance estimates of ET based on flux tower measurements are available for a network of sites in the Arctic and subarctic land areas. Many of these are accessible from the archives of the AmeriFlux database, hosted by the U.S. Department of Energy's Lawrence Berkeley Laboratory (<http://ameriflux.lbl.gov/>). The eddy covariance estimates of the fluxes of moisture (as well as energy and trace gases such as CO<sub>2</sub>) are based on measurements made several meters to tens of meters above the surface (Figure 42). In addition to instrumentation for measuring vertical fluxes, the towers include measurements of temperature and precipitation, enabling evaluations of the relationships between ET, P, and T presented in Section 5. The horizontal footprint of the measurements is typically several tens to 100-200 meters, so the measured fluxes are representative of vegetation in the immediate vicinity of the measurement site. However, one of the main limitations of a comparison of tower measurements and climate model output is that the footprint of the tower measurements is orders of magnitude smaller in scale than the grid cells of climate models. For this reason, we stress the relationships between ET flux variations and the associated drivers (T and P) computed separately from each of the two information sources. ~~Recognizing the~~The scale discrepancy, ~~we also choose for our comparison~~is also the main motivation for our use of a regional climate model ~~with higher resolution~~rather than ~~a~~ global climate models ~~(Section 2.2)~~.

Despite the scale discrepancy, several recent studies have compared tower measurements of ET with corresponding model output. Yao et al. (2016) evaluated ET fluxes simulated by global climate models (with resolutions of 100-200 km) against tower measurements at 240 globally

distributed sites. The aggregate statistics computed by Yao et al. were heavily weighted towards the stations outside the Arctic. Tower measurements at Canadian sites were used by Wang et al. (2015) in a Canada-wide comparison with water budgets, remote sensing products and a land surface models. These studies did not address relationships between ET and the driving variables. These relationships are the focus of the present paper.

In order to assess the moisture fluxes and their drivers across Arctic and subarctic biomes, we present results for a set of four locations in Alaska: two on the tundra (Barrow and Imnavait Creek) and two in the boreal forest (Bonanza Creek and Poker Flat). Figure 2-3 shows the locations of the four sites. The Barrow site is located at the Barrow Environmental Observatory approximately midway between Barrow on the Chukchi Sea coast and the Beaufort Sea (Eilson Lagoon). The coastline is about 3 km to the northeast and 5 km to the northwest of the tower site. Winds from the west, north, and east are onshore, advecting marine air over the site; northeast winds predominate during the summer. The tundra vegetation at Barrow is a mixture of vascular plants such as sedge and nonvascular constituents such as moss and lichens.

The Imnavait site is approximately 200 km south of the Arctic Ocean at the base of the foothills of the Brooks Range near the Arctic Long-Term Ecological Research (LTER) field station at Toolik Lake. While maritime air occasionally impacts the site during summer, the climate is considerably warmer than at Barrow: annual (summer) temperatures are -8°C (+9°C) at Toolik/Imnavait and -11°C (+4°C) at Barrow. Cloudiness is also less pervasive at Imnavait than at Barrow. We use data from two flux tower sites at Imnavait. The 200 m footprint of the “sedge” site, located in the valley bottom, is classified as 52% wet sedge and 47% tussock tundra, with the remainder bare soil or open water. The footprint of the “heath” site is classified

249 as 20% heath, but also includes 72% tussock tundra, with the balance made up of sedge meadow  
250 and bare soil. Figure 3 shows the vegetation in the vicinity of the two Imnavait tower sites.

251 Both the two Imnavait sites and the Barrow site are underlain by continuous permafrost that  
252 is several hundred meters deep. During summer the maximum active layer depths are  
253 approximately 40-60 cm at the Imnavait sites and 20-30 cm at Barrow. Snow typically covers  
254 the ground from October through May, with typical snow depths of 30-40 cm at the start of the  
255 spring thaw, although considerable blowing and drifting results in a heterogeneous distribution  
256 of snow depths.

257 The boreal forest tower sites are at Bonanza Creek and Poker Flat, located about 30 km  
258 southwest and 50 km northeast of Fairbanks, respectively. Both locations are considerably  
259 warmer than the tundra sites in summer, with June-August mean temperatures of approximately  
260 15°C. Winter temperatures are comparable to those at the tundra sites, although with  
261 considerably less wind, and the spring snowmelt occurs 4-6 weeks earlier than on the ~~tundra~~  
262 tundra. The Bonanza Creek tower, part of the Bonanza Creek LTER, is located in a lowland area  
263 underlain by permafrost. The vegetation is mature black spruce forest on a permafrost plateau  
264 (Figure 3). Poker Flat is an upland area of discontinuous permafrost, although the tower itself is  
265 underlain by permafrost. Black spruce is the dominant vegetation type, ~~although there are with~~  
266 some white spruce and birch in the area.

267 For purposes of this study, a key limitation of the tower measurements is the lack of useful  
268 data during the winter months when snow and icing preclude measurements of P and ET. For  
269 this reason, our study focuses on the warm season, May through September, when the full suite  
270 of measurements (T, P, ET) can be documented, analyzed, and compared with the model output.

## ~~2.2 Regional climate model output~~

Global model output is available from several dozen climate modeling centers, and the hydrologic output from the current generation of these models (CMIP5, Coupled Model Intercomparison Project, version 5) has been evaluated by Rawlins et al. (2010), Laine et al. (2014) and Yao et al. (2016). For comparison with site-specific measurements such as those in Section 2.1, finer resolution of model output is highly desirable. Dynamical downscaling by a regional climate model can achieve finer resolution by approximately an order of magnitude. In this study, we analyze P, T, and ET from a widely used regional climate model, the Advanced Research (ARW) core of the Weather Research and Forecasting (WRF) model (Skamarock et al. 2008). The model makes use of a thermodynamic sea ice model (Zhang and Zhang 2001) and the Noah land surface model (Yang et al., 2011) used within WRF in order to model the thermal conditions at the surface. It is driven at the lateral boundaries by observationally based reanalysis fields (ERA-Interim) in order to avoid introduction of additional biases arising from the driving model. The ERA-Interim reanalysis was selected as it has been successfully downscaled using WRF in other regions of the world (e.g. Gao et al. 2015; Srivastava et al. 2014, 2013; Soares et al. 2012), has been used in previous Arctic WRF simulations and analyses (e.g. Liu et al. 2014) and is among the best performing reanalysis data sets for Alaska (Lader et al. 2015) and the wider Arctic (Lindsay et al. 2014).

As described by Bieniek et al. (2016), the downscaling covered a domain with 262x262 grid points that encompassed all of Alaska and portions of far eastern Russia and northern Canada at 20 km horizontal resolution (Figure 4) with 49 vertical model levels. The model was reinitialized every two days and was integrated for a total of 54 hours after each reinitialization. Each initialization occurred at 18 UTC (09 AKST). After each reinitialization, the first 6 hours

of output (a “spin-up” overlapping with the final 6 hours of the previous 54-hour integration) were discarded. The frequent reinitialization to the ERA-Interim reanalysis, together with a continuous nudging to the ERA-Interim upper air fields during each 54-hour simulation, ensured that the model was tightly constrained by the observationally-based reanalysis.

The output from the 2-day simulations was combined together to form the final downscaled product, which spanned the 1979–2015 period. Hourly WRF output was saved and used to produce daily mean values of downscaled variables. The daily ET values were calculated from the daily values of latent heat flux in the archive of model output. (The same conversion was performed with the eddy covariance measurements). The daily mean values of T, P, and ET from the model’s 20-km grid cells corresponding to the tower sites of Section 2.1 were extracted for the years of the available tower data (Section 3).

### 9.3. Methods

The flux tower data were downloaded as 30-minute means that are processed from the high frequency (e.g., 10 Hz) eddy covariance measurements. The data for Barrow and Poker Flat were obtained from the AmeriFlux archive (<http://ameriflux.lbl.gov>), which is maintained by Lawrence Berkeley Laboratory. The Imnavait and Bonanza Creek data were downloaded from the Arctic Observing Network archive maintained by the Institute of Arctic Biology of the University of Alaska, Fairbanks, <http://aon.iab.uaf.edu/>. The measurements and data processing are described in more detail for Imnavait by Euskirchen et al. (2017) and for Bonanza Creek by Euskirchen et al. (2014). For all the sites, the 30-minute values were aggregated into 24-hour values (averages for T; totals for P, and ET) using MATLAB. In the summation of the 30-minute P and ET into daily values, a missing 30-minute value was counted as zero.

Formatted: Indent: Left: 0", Numbered + Level: 1 +  
Numbering Style: 1, 2, 3, ... + Start at: 2 + Alignment: Left +  
Aligned at: 0.25" + Indent at: 0.5"

316 Because the measurements from the tower sites are subject to instrumental outages and  
317 occasional malfunctions, it was necessary to perform several layers of quality-control. The  
318 quality-control procedure was applied to the warm-season months (May through September),  
319 which are the months with above-freezing mean air temperatures and with most of the yearly ET,  
320 as shown in Section 4. First, if occasional 30-minute segments of a day were missing (e.g., ET  
321 data during periods of rain), the daily values were computed as means of all 30-minute values  
322 that were available for the day. Second, we omitted a site-year if one or more of the sensors were  
323 inoperative, were known to be miscalibrated or repeatedly reported values out of range during a  
324 particular year. The years that survived this stage of the quality control are listed in Table 1. It is  
325 apparent that the available data from the various sites span different time periods. Such  
326 differences in temporal coverage, which are characteristic of eddy covariance sites operated  
327 worldwide, result from the diversity of the operators and funding sources of flux tower sites.

328 A special case of the quality-control was the precipitation at the Imnavait site, where three  
329 gauges (tipping buckets) were located within a 1 km<sup>2</sup> area. Calibration and malfunction issues  
330 led to sufficiently long and frequent gaps in the three sets of reliable precipitation measurements  
331 that it was necessary to combine the precipitation records from the three gauges. This  
332 consolidation utilized the most reliable single-gauge value that was available for each day.  
333 ~~Analysis indicated that when~~When data were available from all three precipitation gauges,  
334 ~~analysis indicated~~that the measurements were equivalent as they were all within the same 1 km<sup>2</sup>  
335 area.

336 For the site-years that were retained, data were missing for some days or for some longer  
337 periods. If the gap was only a day or several days, the missing values were interpolated from  
338 available values for surrounding days. For longer intervals (e.g., 5-15 days) of missing

339 temperature and/or precipitation data, values were substituted from nearby station data: the  
340 Barrow airport data were used for the Barrow tower site, and the Fairbanks airport data for the  
341 Bonanza Creek and Poker Flat sites. No such substitution was possible for the Imnavait sites  
342 because there is no nearby reporting station. For the yearly accumulations of P, T, and ET  
343 described in Section 4, the values for a site-year are labeled as “estimated” if more than 45% of  
344 the daily values for May-September were filled in by interpolation or station-substitution.

345 In order to evaluate relationships between ET, T, and P, cross-correlations were evaluated at  
346 various lags (including zero). These cross-correlations, which are presented in Section 4, were  
347 based on departures from the daily averages for each site. The daily averages were computed  
348 using all available years of data for a site, but were replaced by 15-day running means of the  
349 single-date averages. The 15-day running means were used because the relatively small sample  
350 (< 10 years) for each site results in “climatological” seasonal cycles characterized day-to-day  
351 jumps. In the case of temperature, for example, the period-of-record means of the unsmoothed  
352 daily temperatures sometimes ~~varied-can vary~~ by 2° to 3°C from one day to the next.

353 The model output from the simulation described in Section 2.2.1 was available through  
354 2015. The model output was obtained as daily totals of P and ET (and daily averages of T), so  
355 there was no need for infilling of missing values, averaging of 30-minute values, nor correcting  
356 for instrumental malfunctions. For comparison with the in situ measurements, the values of T, P,  
357 and ET for the model grid cells containing the tower sites were extracted for the years  
358 corresponding to the available tower data.

#### 359 4.4. Seasonal and interannual variations

**Formatted:** Font: (Default) Times New Roman, 12 pt, Bold  
**Formatted:** Indent: Left: 0", Hanging: 0.19", Numbered +  
Level: 1 + Numbering Style: 1, 2, 3, ... + Start at: 2 +  
Alignment: Left + Aligned at: 0.25" + Indent at: 0.5"



In the following sections, we present comparisons of the simulated values and the corresponding measurements. Because the results include four variables (ET, P, P-ET and T), four measurement sites (including one with flux towers in two vegetation sites), two sources of each variable for each location, and seasonal climatologies in addition to variations over timescales from daily to seasonal, it is not feasible to present graphical displays of all results for all sites. Therefore, several of the following figures are based on samples of results chosen because they convey the most information relevant to the regional climate model performance. A more comprehensive diagnostic assessment focused on hydrologic processes rather than model evaluation would require additional figures as additional sites and will be pursued in future work.

Sample time series of monthly values illustrating the key features of the ~~measured and model-derived~~ model-derived and measured T, P, ET, and P-ET are shown for the tundra sites in Figure 5 and the forest sites in Figure 6. In each figure, the corresponding time series from the model (blue) can be compared with the tower measurements (red) ~~can be compared with the model's values (blue)~~ for the grid cell containing the tower site. All the measured variables (T, P, ET) undergo strong seasonal cycles, which have larger amplitudes than the interannual variations. It is apparent from Figures 5a and 6a that the seasonal cycles of temperature are well simulated by the model, although the model's temperatures tend to be too high by several degrees during summer at Barrow.

The interannual variations in Figures 5a and 6a show generally good correspondence between the model and the measurements ~~and the model~~, although there are discrepancies, especially in the summer temperatures at Barrow. Because the model was forced by observed lateral and ocean surface/sea ice boundary conditions and was also reinitialized to observational data over Alaska at 48-hour intervals, the year-to-year (and day-to-day variations in the model

383 output should, in principle, agree with the corresponding variations in the measurements. Model  
384 errors (resolution-related as well as formulational) and measurement limitations cause the values  
385 from the two sources to differ. In the case of the Barrow temperatures, the discrepancies are also  
386 attributable to the proximity of the Barrow tower to the coastline (and onshore advection of cool  
387 maritime air during summer), while the model's temperatures for the Barrow grid cell are  
388 averages for a land area 20 km on a side.

389       The comparison of measured and model-derived precipitation is limited to the warm season  
390 because, as noted earlier, the instrumentation at the tower sites does not enable meaningful  
391 estimates winter precipitation amounts. Winter values of P are therefore shown as zero in Figures  
392 5 and 6. However, Figures 5b and 6b show that the models over-simulate warm-season  
393 precipitation by a significant amount. The interannual variations of P are captured to some extent  
394 at the Poker Flat forest site, especially the extremely wet year of 2014, but there is little  
395 correspondence between the interannual variations of measured and modeled P at Barrow.  
396 However, the ET variations at Imnavait (Figure 5c) show generally good correspondence  
397 between the model and the measurements, including the interannual variations. Figure 5c also  
398 shows that ET is similar at the sedge and heath sites in terms of both the mean seasonal cycle and  
399 the interannual variations, although the interannual variations at the sedge site are somewhat  
400 closer to the model's values. The most notable discrepancy between the model and the  
401 measurements at Imnavait is in the net surface flux, P-ET (Figure 5d). The model's P-ET  
402 generally remains positive throughout the summer, except for single-month excursions that  
403 barely reach into negative values in a few years. The measurements, on the other hand, show  
404 stronger excursions into negative P-ET (net moisture loss), often for more than one month, at  
405 both tower sites, especially at the sedge site. In only one year (2014) of the eight years of

406 measurements did the monthly tower-derived ET remain positive through the summer. The  
407 model's excessive summer wetness (positive P-ET) is attributable to the model's much larger P  
408 relative to the in situ measurements, as the differences in ET are not as large.

409 At the forest sites, the model shows greater P as well as greater ET relative to the  
410 observations (Figure 6). The over-simulations of P and ET act to offset each other somewhat,  
411 resulting in warm-season P-ET that is comparable in the model and the data, with more than one  
412 month of drying (negative P-ET) indicated by each source in most years. Figure 6d even shows  
413 some model-data correspondence in the interannual variations of P-ET. 2013 and 2015 were  
414 relatively dry years according to both sources of information.

415 The biases of the model are clearly apparent in the monthly means of the hydrologic  
416 variables, which are shown in Figure 7 for Barrow and Poker Flat. The results for Imnavait and  
417 Poker Flat (not shown) are similar. P and ET are over-simulated by the model in all months for  
418 which the tower data are available, and the over-simulation is greater in the boreal forest than on  
419 the tundra. The excess ET in the model is almost certainly driven in part by the excess P,  
420 although the model-data discrepancies in ET at Barrow are larger than the model-data  
421 discrepancies in P at Barrow. Figure 7 also makes the point that, *in the model*, the cold-season  
422 fluxes are much smaller than the warm-season fluxes, especially in the boreal forest. The tower  
423 data do not permit summer-winter comparisons of P or ET.

424 The climatological (mean over all years) seasonal cycles of P-ET, the net surface moisture  
425 flux, show interesting differences among the various sites and in the model's ability to capture  
426 the seasonal cycle of P-ET. As shown in Figure 8a, there is a net moisture loss during June and  
427 July at the Barrow tower site and during June at the Imnavait tower sites. The differences

428 between the two Imnavait sites are small in all calendar months. However, there are large  
429 discrepancies between the P-ET of the model and the tundra tower sites. Figure 8a shows that  
430 the model's summer P-ET is much more negative than the tower-derived values at Barrow, and  
431 much more positive than the tower-derived values at Imnavait. In other words, the model shows  
432 excessive summer drying at Barrow and excessive summer wetting at Imnavait. The excess  
433 drying at Barrow is attributable to the model's excess warmth at Barrow (Figure 5a), while the  
434 model's excess wetting at Imnavait is attributable to the model's excessive precipitation (Figures  
435 5c and 5d). These different reasons for the model's biases in the critical quantity, P-ET, point to  
436 the challenges in obtaining credible model simulations of the surface moisture budget in Arctic  
437 tundra regions.

438 Figure 8b shows the corresponding P-ET climatologies for the forest sites, for which the  
439 model and the measurements are in surprisingly good agreement – given the discrepancies in the  
440 simulated and measured P. The outstanding feature of Figure 8b is the difference in sign  
441 between summer P-ET at the two sites: a net moisture loss at Bonanza Creek and a net moisture  
442 gain at Poker Flat in both the model output and the tower data. This difference is consistent with  
443 greater subsurface moisture storage at Poker Flat, where the active layer is deeper and the  
444 permafrost is discontinuous. However, an additional factor contributing to the difference is the  
445 inclusion of a very high precipitation year, 2014 (Fig. 6b) in the climatology for Poker Flat but  
446 not for Bonanza Creek. While Bonanza Creek's P was available for 2014 (and was well above  
447 its mean, as shown in Section 5.1), ET was not available because of an instrument outage.  
448 Hence P-ET could not be included in the Bonanza Creel multiyear averages in Figure 8b.

#### 449 **11.5. Relationships to atmospheric drivers**

Formatted: Indent: Left: 0", Numbered + Level: 1 +  
Numbering Style: 1, 2, 3, ... + Start at: 2 + Alignment: Left +  
Aligned at: 0.25" + Indent at: 0.5"

450 In order to assess the linkages between ET and two of its key drivers (T and P), we focus on  
451 variations over two timeframes: (1) yearly totals, computed as accumulations over the June-  
452 September “warm season” when the ground is generally snow-free and ET is largest, and (2)  
453 variations of ET over short periods of one to several days.

#### 454 5.1 Warm-season integrals of ET and drivers

455 5.1.1 Seasonally accumulated totals of ET provide a means to evaluate the relationships  
456 between interannual variations of ET and its drivers. In this section we present accumulation  
457 curves for the different variables based on observational measurements in order to provide  
458 estimates unaffected by model biases. We then correlate the interannual variations of the  
459 seasonal totals of E and ET with corresponding totals of precipitation and temperature anomalies  
460 in order to assess the relative contributions of T and P to the ET and P-ET. Finally, we compare  
461 correlations based on the model-output and the on the observational measurements in order to  
462 assess the model’s ability to capture the drivers of interannual variations of ET and P-ET.

463 Warm-season accumulations of (a) daily temperature anomalies, (b) precipitation, and (c)  
464 ET are shown in Figures 9 for a tundra site (Imnavait heath) and in Figure 10 for a forest site  
465 (Bonanza Creek). In all cases, the summations are performed for the four-month period June 1  
466 through September 30. The accumulated temperature anomalies in Figure 9 show that some  
467 years at Imnavait were relatively warm (2010, 2012), while others were relatively cool (2014,  
468 2015). For scaling purposes, we note that a 4-month accumulated temperature departure of 122°C  
469 corresponds to a seasonally averaged departure of 1°C. 2015’s value of -210°C in Fig. 9a  
470 therefore represents a summer temperature departure of approximately -1.7°C (-3.1°F). Figure  
471 9b shows that the wettest year (2012) had more than twice the precipitation of the driest year

Formatted: Indent: Left: 0.06", Hanging: 0.19", Outline numbered + Level: 2 + Numbering Style: 1, 2, 3, ... + Start at: 1 + Alignment: Left + Aligned at: 0.25" + Indent at: 0.5", Tab stops: 0.38", Left + 0.44", Left

Formatted: No bullets or numbering

Formatted: Font: Not Italic

(2013). Examination of Figure 10c shows that 2009 and 2010 (warm years) were the years with the greatest ET, while 2015 (a cool year) was the year with the smallest ET.

Table 2 lists the correlations (across the available years) between the warm-season totals of P, E, P-E and the T anomaly. The table includes values computed from the model simulations for the same years, enabling a comparison of the relative importance of T and P for the hydrologic fluxes, ET and P-ET. Figure 11 is a graphical comparison of the measurement- and model-based correlations for the Imnavait and Bonanza Creek sites, highlighting the model's ability to capture the contributions of T and P to the interannual variations at the sites with the most coherent signals between the atmospheric and hydrologic variables. For the observational results, the When the full set of years is considered, the correlations between seasonally accumulated T and total ET at the Imnavait heath site is 0.63, sites are 0.63 (heath) and 0.71 (sedge), indicating that seasonally integrated evapotranspiration tends to be greater in warmer years and smaller in cooler years. This correlation is based on an admittedly small sample of nine years, but it is even larger for the Imnavait wet sedge site and in the model output for Imnavait (Figure 11). The corresponding value is 0.77 for the model's 20 km x 20 km Imnavait grid cell, which contains both heath and sedge tundra. For the sample size of N = 9 (years), the 95% significance level is approximately 0.69, so the correlations obtained from the sedge measurements and the model simulation are statistically significant despite the small sample size.

By contrast, there is little correspondence between the seasonally accumulated P and seasonal ET: the correlations between the yearly P and ET at Imnavait are -0.13-12 (heath measurements) and -0.40-48 (sedge measurements), and -0.24 (model), none of which are statistically significant. We conclude that the primary driver of interannual variations of total warm-season ET at Imnavait is temperature. The implication is that a warming climate will lead to greater ET,

even if P also increases in a warming climate as projected by global models. However, the measurements from Barrow show no meaningful correlation between T and ET, but a strongly negative correlation between P and ET. Given the saturated surface conditions at Barrow, this negative correlation with P may point to the tendency for ET to be greater when cloudiness is reduced, allowing for greater insolation. This hypothesis is speculative and requires further examination with additional data (radiative fluxes and winds).

At the forest sites, there is also a positive correlation between seasonally integrated measurements of T and ET ( $r = +0.67$  at Bonanza Creek,  $r = +0.76$  at Poker Flat). The corresponding model-derived values are  $+0.58$  and  $+0.81$ . At Bonanza Creek, ET correlates even more strongly with P ( $r = +0.73$ ) than with T, pointing to a role of recycling of moisture through ET. ~~This~~ However, this signal is not apparent at Poker Flat, ~~where there are only four years of reliable ET measurements~~ nor in the model results for either forest site.

A universal feature of the measurement- and model-derived results for all four sites is the strong positive correlation ~~However, there are strong correlations~~ between seasonal totals of P and P-ET ~~at the forest sites~~ (Table 2 and Figure 11). While the inclusion of P in P-ET virtually guarantees some correlation, the magnitudes of the P vs. P-ET correlations ( $>0.9$  in most cases) indicates that the effects of temperature ~~(negatively correlated with P,  $r = -0.55$ )~~ do little to offset the effects of P on surface moisture exchange. Figure 11 shows that the model also reproduces the high correlation between seasonally integrated P and P-ET at Bonanza Creek despite the model's strong correlation between T and P-ET,  $r = -0.88$ , which is much more negative than in the tower data. Even at the tundra sites, the seasonally integrated P-ET correlates more strongly with P than with T, despite the strong dependence of ET on T. We conclude that precipitation is the main driver of P-ET at all sites on a year-to-year basis, implying that future changes of the

surface moisture budget will be determined by future changes in P more than by changes in T.

The robustness of this conclusion is supported by the consistency between the model results and *in situ* measurements.

Formatted: Font: Italic

## 5.2 Short-term variations of ET and its drivers

—The seasonal relationships summarized in the previous subsection represent integrations of shorter-term linkages between ET and its drivers, T and P. In order to quantify the shorter-term linkages, we computed cross-correlations between ET and T as well as ET and P with the variables averaged over periods of 1, 3 and 30 days. We show the results as cross-correlation functions of lead/lag, whereby the ET leads or lags the T and P variations by 0, 1, 2, ..., 30 days. Figure 12 shows these cross-correlation functions computed from the daily values of T, P, and ET for Imnavait Creek, Bonanza Creek and Poker Flat. Results are shown for both the tower data (solid lines) and the model (dashed lines). In all cases, the daily values have been converted to departures from the daily means, thereby removing the effects of the seasonal cycle from the correlations.

Two peaks appear consistently in the correlation functions: a positive correlation of ET with temperature, centered at or close to zero lag, and a negative correlation of ET with precipitation, also centered at zero lag. The positive temperature correlation is consistent with the seasonal results in Section 5.1: ET is greater when the temperature is higher than its daily average. The correlation functions for temperature decay rapidly on either side of lag zero, although the values still stand out above the noise-level at temperature leads and lags of a day or two, consistent with the autocorrelations of daily temperature anomalies. The zero-lag correlations between T and ET are slightly stronger in the model ( $r = +0.4$  to  $+0.5$ ) than in the tower data ( $r = +0.3$  to  $+0.4$  at



540 Imnavait and Bonanza Creek), in agreement with the relative strength of the seasonal  
541 correlations between T and ET in Figure 11 [and Table 2](#). The lower zero-lag correlations at  
542 Barrow suggest that the high humidity and cloud coverage limit the importance of air  
543 temperature in daily variations of ET.

544 The zero-lag peaks in Figure 12's correlations between P and ET are weaker than those of the  
545 temperature correlations. The negative sign of the zero-lag spikes is not attributable to a direct  
546 effect of falling precipitation, as the eddy covariance fluxes during precipitation events have  
547 removed from the database because the measurements are problematic when the instruments are  
548 wet. The most plausible explanation for the negative peaks at zero-lag is that temperatures tend  
549 to be depressed on days with precipitation and clouds, so the negative spikes in the P curves may  
550 actually be indirect manifestations of the temperature correlations. The fact that the Imnavait  
551 correlations with ET are larger for both T and P at the sedge site compared to the heath site  
552 supports the connection between the two drivers. Aside from the spike at zero lag, precipitation  
553 shows little association with ET, consistent with the seasonal results presented earlier.

554 While the short-term associations with T and P are largest at zero lag, one may hypothesize  
555 cumulative effects of T or P anomalies may cause a stronger signal if the T vs. ET and P vs. ET  
556 relationships are evaluated over timescales longer than a day (Figure 12) but shorter than a  
557 season (Figure 12). To test this hypothesis, we experimented with the use of running means of  
558 T, P, and ET in the correlative analysis. The averaging period for the running means varied from  
559 several days to 30 days. Figure 13 shows the correlation functions based on 3-day means for the  
560 two Imnavait sites and the corresponding model output. While the correlation functions decay  
561 from their zero-lag values at a slower rate with the smoothed data, the maximum values are  
562 essentially the same as in Figure 12a. Even the relative magnitudes of the sedge-vs.-heath tundra

563 and measurement-vs.-model peaks are little changed from the results based on single-day values.  
564 Experiments with longer averaging periods produced no enhancement of the associations and  
565 even led to a degradation of the correlations as the averaging period approached 30 days. We  
566 conclude that any multiday cumulative effects are not strong enough to enhance the concurrent  
567 (zero-lag) associations inherent in the daily data.

## 568 12.6. Conclusion

569 The results in the preceding sections lead to the following conclusions:

570 Both P and ET are considerably larger in the model for all sites, indicating that the model's  
571 hydrological cycle is stronger than the observed. This over-simulation of the high-latitude  
572 hydrologic cycle is consistent with the known tendency of global models to simulate more  
573 precipitation than is observed in northern high latitudes (Walsh et al., 2002; de Boer et al.,  
574 2012), subject to uncertainties in the observational data.

575 •

576 The model output and the tower measurements from all sites show a short period (one or  
577 two months) of negative P-ET during summer, indicative of surface drying, although the  
578 model does not show this period of drying ~~in at~~ the Imnavait tundra sites in the foothills of  
579 the Brooks Range.

581 At all sites, interannual variations in the warm-season surface water balance (P-ET) are  
582 determined primarily by variations in precipitation. The dominance of P as a driver is  
583 especially apparent at the forest sites, and it is apparent in the model output as well as in the  
584 observational data.

Formatted: Indent: Left: 0", Numbered + Level: 1 +  
Numbering Style: 1, 2, 3, ... + Start at: 2 + Alignment: Left +  
Aligned at: 0.25" + Indent at: 0.5"

Formatted: List Paragraph, Indent: Left: 0.04", Bulleted +  
Level: 1 + Aligned at: 0.06" + Indent at: 0.33"

Formatted: Font: (Default) Times New Roman, 12 pt

Formatted: List Paragraph, Indent: Left: 0.31"

Formatted: Font: (Default) Times New Roman, 12 pt

Formatted: Normal, Indent: Left: 0", Hanging: 0.31", No  
bullets or numbering

Formatted: Font: (Default) Times New Roman, 12 pt

Formatted: Font: (Default) Times New Roman, 12 pt

Formatted: Normal, Indent: Left: 0", Hanging: 0.25",  
Space After: 0 pt

• At both the Imnavait tundra and Poker Flat forest sites, the model and the measurements are consistent in showing that variations of evapotranspiration are controlled primarily by temperature. The dominance of temperature as a driver is supported especially by the interannual variations of the seasonal totals, but also by correlations on the daily timescale, in both the model results and the observational data. Only the model shows this dominance of temperature at the Barrow tundra and Bonanza Creek forest sites.

~~• At all sites, interannual variations in the warm-season surface water balance (P-ET) are determined primarily by variations in precipitation. The dominance of P as a driver is especially apparent at the forest sites, and it is apparent in the model output as well as in the observational data.~~

~~• Both P and ET are considerably larger in the model for all sites, indicating that the model's hydrological cycle is stronger than the observed. This over-simulation of the high-latitude hydrologic cycle is consistent with the known tendency of global models to simulate more precipitation than is observed in northern high latitudes (Walsh et al., 2002; de Boer et al., 2012), subject to uncertainties in the observational data.~~

~~Taken at face value, the results imply that a warming climate will lead to greater warm-season ET at tundra sites because summers will be warmer and longer. At all sites, however, the seasonal net surface water flux (P-ET) is more sensitive to precipitation than to temperature,~~

Formatted: Indent: First line: 0"

608 ~~implying that future changes in atmospheric exchanges with the land surface will be largely~~  
609 ~~controlled by changes in precipitation. Such findings are based on a small sample of only two~~  
610 ~~tundra and two forest locations and fewer than ten years of data for each location, so they are~~  
611 ~~largely exploratory. Furthermore, changes in actual wetness of the ground surface will also~~  
612 ~~depend on future changes in active layer and surface drainage, which may be affected by~~  
613 ~~thermokarst in areas of permafrost thaw.~~

614 Given the small sample of locations and years, a high priority is the extension of this evaluation  
615 to other high-latitude sites. Existing flux data networks (AmeriFlux, FluxNet) contain several  
616 dozen Arctic or subarctic stations with record lengths spanning several years to a decade or  
617 more. A related need is to address the uncertainties in the precipitation data. Precipitation is  
618 notorious for small-scale variations as well as instrumental challenges (e.g., gauge undercatch),  
619 so the robustness of conclusions based on precipitation data is open to question.

620 Finally, ~~t~~The discrepancies between the tower and model values of P and ET found here are  
621 sufficiently large that there is a need to determine whether other models show similar biases. A  
622 related need is to address the uncertainties in the precipitation data. Precipitation is notorious for  
623 small-scale variations as well as instrumental challenges (e.g., gauge undercatch), so the  
624 robustness of conclusions based on precipitation measurements is open to question.~~The WRF~~  
625 ~~model may or not be an outlier in this regard. Whether or not it is, the reasons for the~~  
626 ~~discrepancies need to be explored in terms of the processes included in the land model and the~~  
627 ~~parameterizations used to represent key processes related to evapotranspiration.~~

628 Taken at face value, the results imply that a warming climate will generally lead to greater  
629 warm-season ET at tundra sites because summers will be warmer and longer. At all sites,  
630 however, the seasonal net surface water flux (P-ET) is more sensitive to precipitation than to

Formatted: List Paragraph

631 temperature, implying that future changes in atmospheric exchanges with the land surface will be  
632 largely controlled by changes in precipitation. Such findings are based on a small sample of only  
633 two tundra and two forest locations and fewer than ten years of data for each location, so they are  
634 largely exploratory. Furthermore, changes in actual wetness of the ground surface will also  
635 depend on future changes in active layer and surface drainage, which may be affected by  
636 thermokarst in areas of permafrost thaw. Such processes are not yet included in most climate  
637 models. Because models will continue to be the primary tools for anticipating future changes, it  
638 is important that Arctic terrestrial simulations be extended to additional models, especially as  
639 models evolve to include additional processes relevant to Arctic terrestrial hydrology.

640

#### 641 **ACKNOWLEDGMENTS**

642 Ross Fischer was supported by the National Science Foundation (NSF) through Grant ARC-  
643 1560372, an REU (Research Experience for Undergraduates) grant to the University of Alaska,  
644 Fairbanks. Funding for the eddy covariance data collection at the Imnavait flux tower sites was  
645 through the NSF Division of Polar Programs, Arctic Observatory Network grant numbers  
646 1503912, 1107892 and 0632264. Funding for the Bonanza Creek flux tower measurements was  
647 provided by the NSF through the Bonanza Creek Long Term Ecological Research Program and  
648 the U.S. Geological Survey.

649

## REFERENCES

- Bieniek, P. A., U. S. Bhatt, J. E. Walsh, T. S. Rupp, J. Zhang, J. R. Krieger, and R. Lader, 2015: Dynamical downscaling of ERA-Interim temperature and precipitation for Alaska. *J. Appl. Meteor. Climatol.*, 55(3), 1276-1289, DOI: 10.1175/JAMC-D-15-0153.1.
- Bring, A., I. Federova, Y. Dibike, L. Hinzman, J. Mard, S. H. Mernild, T. Prowse, O. Semenova, S. L. Stuefer, and M.-K. Woo, 2016: Arctic terrestrial hydrology: A synthesis of processes, regional effects, and research challenges. *J. Geophys. Res.: Biogeosciences*, doi: 10.1002/2015JG003131.
- de Boer, G., W. Chapman, J. E. Kay, B. Medeiros, M. D. Shupe, S. Vavrus, and J. Walsh, 2012: A characterization of the present-day Arctic atmosphere in CCSM4. *J. Climate*, 25, 2676-2691.
- Dirmeyer, P. A., Y. Jin, B. Singh, and X. Yam, 2013: Trends in land-atmosphere interactions from CMIP5 simulations. *J. Hydrometeorology*, 14(3), 829-849.
- Euskirchen, E. S., M. S. Bret-Harte, G. R. Shaver, C. W. Edgar, and V. E. Romanovsky, 2017: Long-term release of carbon dioxide from arctic tundra ecosystems in northern Alaska. *Ecosystems*, 20(5), 960-974, doi:10.1007/s10021-016-0085-9.
- Euskirchen, E. S., M. S. Bret-Harte, G. J. Scott, C. Edgar, and G. R. Shaver, 2012: Seasonal patterns of carbon dioxide and water fluxes in three representative tundra ecosystems in northern Alaska. *Ecosphere*, (1):4. <http://dx.doi.org/10.1890/ES11-00202.1>.
- Euskirchen, E. S., C. Edgar, M. R. Turetsky, M. P. Waldrop, and J. W. Harden, 2014: Differential response of carbon fluxes to climate in three peatland ecosystems that vary in the presence and stability of permafrost. *J. Geophys. Res.: Biogeosciences*, 119, 1576–1595, doi:10.1002/2014JG002683.

672

673 Flannigan, M. D., B. M. Wotton, G. A. Marshall, W. J. de Groot, J. Johnston, N. Jurko, and A. S.  
674 Cantin, 2015: Fuel moisture sensitivity to temperature and precipitation: Climate change  
675 implications. *Climatic Change*, doi: 10.1007/s10584-015-1521-0.

676 Gao, Y., J. Xu, and D. Chen, 2015: Evaluation of WRF mesoscale climate simulations over the  
677 Tibetan Plateau during 1979-2011. *J. Climate*, 28, 2823-2841.

678 IPCC, 2013: *Climate Change 2013: The Physical Science Basis*. Report of Working Group 1,  
679 Intergovernmental Panel on Climate Change. Cambridge University Press, Cambridge, U.K.,  
680 1535 pp., doi:10.1017/CBO9781107415324.

681 Lader, R., U. S. Bhatt, J. E. Walsh, T. S. Rupp, and P. A. Bieniek, 2015: Evaluation of  
682 Reanalysis Products for Alaska to Facilitate Climate Impact Studies. *J. Appl. Meteor. Climatol.*,  
683 55(4). 901-922. doi: 10.1175/JAMC-D-15-0162.1.

684 Lafleur, P. M., and E. R. Humphreys, 2007: Spring warming and carbon dioxide exchange over  
685 low Arctic tundra in central Canada. *Global Change Biology*, 14, 740-756.

686 Lafleur, P. M., E. R. Humphreys, V. L. St. Louis, M. C. Myklebust, T. Papakryiakou, L.  
687 Poissant, J. D. Barker, M. Pilote, and K. A. Swystun, 2012: Variation in peak growing season net  
688 ecosystem production across the Canadian Arctic. *Env. Science and Technology*, 46(15), 7971-  
689 7977.

690 Lainé, A., H. Nakamura, K. Nishii, and T. Miyahasaka, 2014: A diagnostic study of future  
691 evaporation changes projected in CMIP5 climate models. *Climate Dynamics*, 42, 2745-2761.

692 Lindsay, R., M. Wensnahan, A. Schweiger, and J. Zhang, 2014: Evaluation of Seven Different  
 693 Atmospheric Reanalysis Products in the Arctic. *J. Climate*, **27**, 2588–2606.

694 Liu F., J. R. Krieger, and J. Zhang, 2013: Toward producing the Chukchi/Beaufort High-  
 695 Resolution Atmospheric Reanalysis (CBHAR) via the WRFDA data assimilation system. *Mon.*  
 696 *Wea. Rev.*, *142*(2), 788-805.

697 Niu, G.-Y., Z.-L. Yang, K. E. Mitchell, F. Chen, M. B. Ek, M. Barlage, A. Kumar, D. Niyogi, E.  
 698 Rosero, M. Tewari, and Y. Xia, 2011: The community Noah land surface model with  
 699 multiparameterization options (Noah-MP): 1. Model description and evaluation with local-scale  
 700 measurements. *J. Geophys. Res.*, *116*, D12109, doi:10.1029/2010JD015139.

701 Ohta, T., T. C. Maximov, A. J. Dolman, T. Nakai, M. K. van der Molen, A. K. Kononov, A. P.  
 702 Maximov, T. Hiyama, Y. Iijima, E. J. Moors, H. Tanaka, T. Toba, and H. Yabuki, 2008:  
 703 Interannual variation of water balance and summer evapotranspiration in an eastern Siberian  
 704 larch forest over a 7-year period (1998-2006). *Agricul. and Forest Meteorol.*, *148*, 1941-1953.

705 Partain, J. L. Jr., S. Alden, U. S. Bhatt, P. A. Bieniek, B. R. Brettschneider, R. T. Lader, P. Q.  
 706 Olsson, T. S. Rupp, H. Strader, R. L. Thoman, Jr., J. E. Walsh, A. D. York, and R. H. Ziel, 2016:  
 707 An assessment of the role of anthropogenic climate change in the Alaska fire season of 2015.  
 708 *Bull. Amer. Meteor. Soc.*, *97*(12), S14-S18.

709 Rawlins, M. A., M. Steele, and 28 coauthors, 2010: Analysis of the Arctic system for freshwater  
 710 cycle intensification: Observations and expectations. *J. Climate*, *23*, 5715-5737.

711 Skamarock, W. C. and Coauthors, 2008: A Description of the Advanced Research WRF Version  
 712 3. NCAR Tech Note, NCAR/TN-475+STR, 113 pp.



713 Soares, P. M. M., R. M. Cardoso, P. M. A. Miranda, J. de Medeiros, M. Belo-Pereira, and F.  
 714 Espirito-Santo, 2012: WRF high resolution dynamical downscaling of ERA-Interim for Portugal.  
 715 *Clim. Dyn.*, *39*, 2497-2522.

716 Srivastava, P. K. D. Han, M. A. Rico-Ramirez, and T. Islam, 2014: Sensitivity and uncertainty  
 717 analysis of mesoscale model downscaled hydro-meteorological variables for discharge  
 718 prediction. *Hydrol. Processes*, *28*, 4419-4432.

719 Srivastava, P. K., D. Han, M. A. Rico, and T. Islam, 2013: Comparative assessment of  
 720 evapotranspiration derived from NCEP and ECMWF global datasets through Weather Research  
 721 and Forecasting model. *Atmos. Sci. Let.*, *14*, 118-125.

722 Walsh, J. E., V. M. Kattsov, W. L. Chapman, V. Govorkova, and T. Pavlova, 2002: Comparison  
 723 of Arctic climate simulations by uncoupled and coupled global models. *J. Climate*, *15*, 1429-  
 724 1446.

725 Wang, S., M. Pan, Q. Mu, X. Shi, J. Mao, C. Brummer, R. S. Jassal, P. Krishnan, J. Li, and T. A.  
 726 Black, 2015: Comparing evapotranspiration from eddy covariance measurements, water budgets,  
 727 remote sensing, and land surface models over Canada. *J. Hydrometeorology*, *16*, 1540-1560.

728 Yao, Y., S. Liang, and 25 coauthors, 2016: Assessment and simulation of global terrestrial latent  
 729 heat flux by synthesis of CMIP5 climate models and surface eddy covariance observations.  
 730 *Agricultural and Forest Meteorology*, *223*, 151-167.

731 Zhang, X. and J. Zhang, 2001: Heat and freshwater budgets and pathways in the Arctic  
 732 Mediterranean in a coupled ocean/sea-ice model. *J. Oceanogr.*, *57*, 207-237.

733

734

735

TABLE 1: Years of available data from each tower site

736

737

Barrow 1998-2007

738

Imnavait Cr. 2007-2015

739

Bonanza Cr. 2010-2013, 2015-2016

740

Poker Flat 2011-2014

741

742

743

744

745

746

747

748

749

750

751

752

753

754

755

756 Table 2. Correlations between total seasonal accumulations of P, ET, P-ET and temperature (T)  
 757 anomaly. Accumulations span June 1 through September 30 as in Figures 9 and 10.

		ET vs. T	ET vs. P	P-ET vs. T	P-ET vs. P
761	<u>Barrow</u> measurements	-0.22	-0.89	0.38	0.98
762	model	0.67	0.13	-0.29	0.86
764	<u>Imnavait</u> measurements (heath)	0.63	0.12	0.43	0.81
765	measurements (sedge)	0.71	-0.48	0.26	0.99
766	model	0.77	-0.24	-0.12	0.97
768	<u>Bonanza Cr.</u> measurements	0.67	0.73	-0.03	0.98
769	model	0.58	-0.07	-0.88	0.89
771	<u>Poker Flat</u> measurements	0.76	-0.39	-0.90	0.99
772	model	0.81	-0.36	-0.91	0.98

Formatted: Indent: Left: 0", Hanging: 0.63", Line spacing: Double

774 **FIGURE CAPTIONS**

775 Figure 41. The domain of the WRF regional climate model simulation. Blue dots are spaced at  
776 intervals of 20 km, the horizontal resolution of the model.

777

778 Figure 42. Flux towers at Poker Flat (left) and Bonanza Creek (right).

779 Figure 23. Locations of the flux tower sites: Barrow and Imnavait Creek on the tundra, and  
780 Bonanza Creek and Poker Flat in the boreal forest.

781 Figure 34. Vegetation in vicinity of flux towers at Bonanza Creek (left) and Imnavait Creek  
782 (right). Imnavait photos show heath tundra (upper right) and wet sedge tundra (lower  
783 right).

784 ~~Figure 4. The domain of the WRF regional climate model simulation. Blue dots are spaced at~~  
785 ~~intervals of 20 km, the horizontal resolution of the model.~~

786 Figure 5. Sample time series of tower measurements (red/yellow) and corresponding model  
787 output (blue) for tundra sites averaged over monthly periods: (a) air temperatures at  
788 Barrow, (b) precipitation, P, at Barrow, (c) evapotranspiration, ET, at Imnavait, with  
789 separate curves for heath tundra (red) and sedge tundra (yellow), and (d) P-ET at  
790 Imnavait, with separate curves for heath and sedge tundra. Note that the towers do not  
791 provide meaningful values of P and ET during the cold season.

792 Figure 6. As in Figure 5, but for forest sites: (a) air temperature at Poker Flat, (b) precipitation,  
793 P, at Poker Flat, (c) evapotranspiration, ET, at Bonanza Creek, (d) P-ET at Bonanza  
794 Creek.

Formatted: Left, Indent: Left: 0", Hanging: 0.69"

795 Figure 7. Monthly climatologies (averages over all available years) of tower measurements  
796 (blue) and corresponding model simulations (yellow) of (a) precipitation at Barrow,  
797 (b) evapotranspiration at Barrow, (c) precipitation at Poker Flat, and (d)  
798 evapotranspiration at Poker Flat.

799 Figure 8. Climatological (average over all available years) monthly values of P-ET at tundra  
800 sites (upper panel) and forest sites (lower panel). Values derived from tower  
801 measurements are shown by solid lines, model-simulated values by dashed lines.

802 Figure 9. Seasonal (June through September) accumulations of (a) air temperature anomalies,  
803 (b) precipitation and (c) evapotranspiration at the Imnavair heath site. All values are  
804 based on tower measurements. Different years are color-coded; dashed lines are  
805 estimated values (see text) for years with large amounts of missing data.

806 Figure 10. As in Figure 9, but for seasonal accumulations at Bonanza Creek.

807 Figure 11. Sample correlations between yearly warm-season totals of ET, P-ET, and driving  
808 variables (T, P). Blue and green bars are correlations based on tower data; yellow  
809 bars are correlations based on model simulation.

810 Figure 12. Cross-correlation functions of daily ET with daily temperature (red) and daily  
811 precipitation (blue) for (a) Imnavait Creek, (b) Bonanza Creek and (c) Poker Flat.  
812 Correlations are plotted as a function of the lag of P and T relative to ET (i.e., T and P  
813 lead ET to the left of zero lag; T and P lag ET to the right of zero lag). Solid lines are  
814 based on tower measurements, dashed lines on model output.

815 Figure 13. As in Figure 12, but for cross-correlations computed from 3-day running means of T,  
816 P, and ET at Imnavait Creek. Solid lines are based on tower measurements, dashed  
817 lines on model output. Values for wet sedge and heath are plotted in different colors.

818



819

820

821 Figure 41. The domain of the WRF regional climate model simulation. Blue dots are spaced at  
822 intervals of 20 km, the horizontal resolution of the model.

823

824

825

826

827

828

829

830

831

832

833

834

835



Poker Flat  
Flux Tower

Bonanza Creek  
Flux Tower



836

837

838

Figure 42. Flux towers at Poker Flat (left) and Bonanza Creek (right).



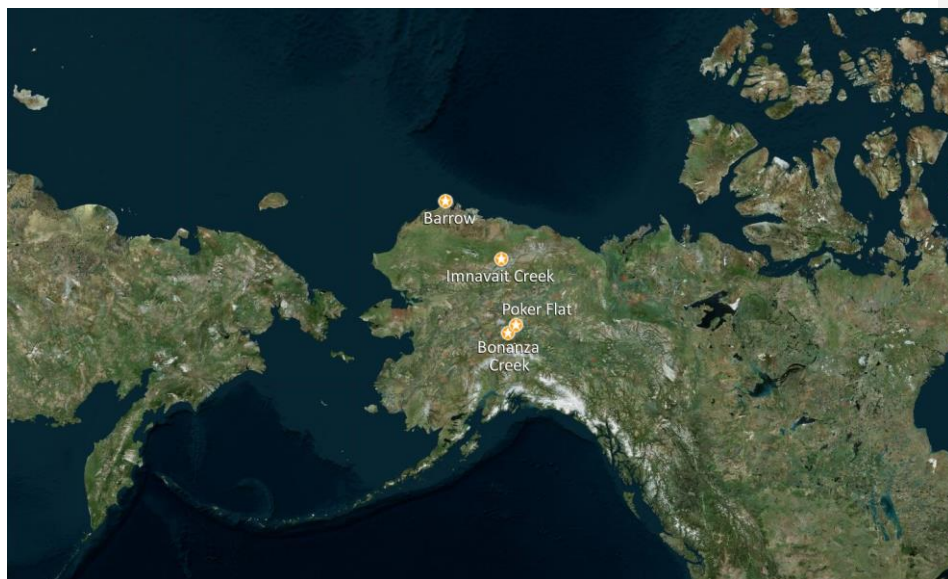


Figure 2.3. Locations of the flux tower sites: Barrow and Imnavait Creek on the tundra, and Bonanza Creek and Poker Flat in the boreal forest.

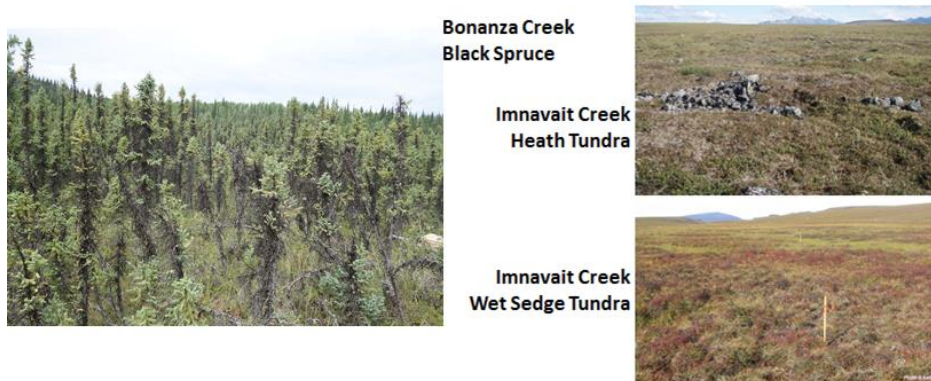


Figure 34. Vegetation in vicinity of flux towers at Bonanza Creek (left) and Imnavait Creek (right). Imnavait photos show heath tundra (upper right) and wet sedge tundra (lower right).



Figure 4. The domain of the WRF regional climate model simulation. Blue dots are spaced at intervals of 20 km, the horizontal resolution of the model.

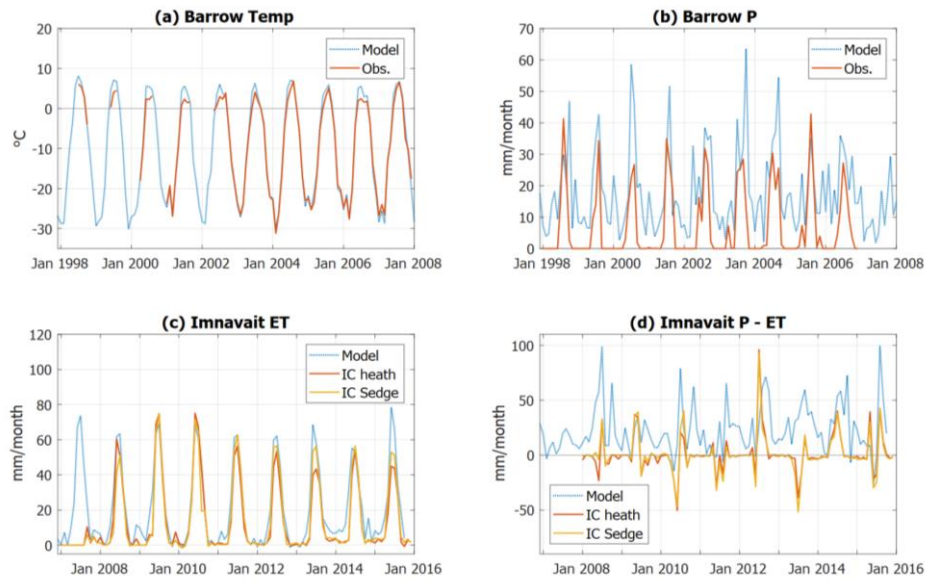


Figure 5. Sample time series of tower measurements (red/yellow) and corresponding model output (blue) for tundra sites averaged over monthly periods: (a) air temperatures at Barrow, (b) precipitation, P, at Barrow, (c) evapotranspiration, ET, at Imnavait, with separate curves for heath tundra (red) and sedge tundra (yellow), and (d) P-ET at Imnavait, with separate curves for heath and sedge tundra. Note that the towers do not provide meaningful values of P and ET during the cold season.

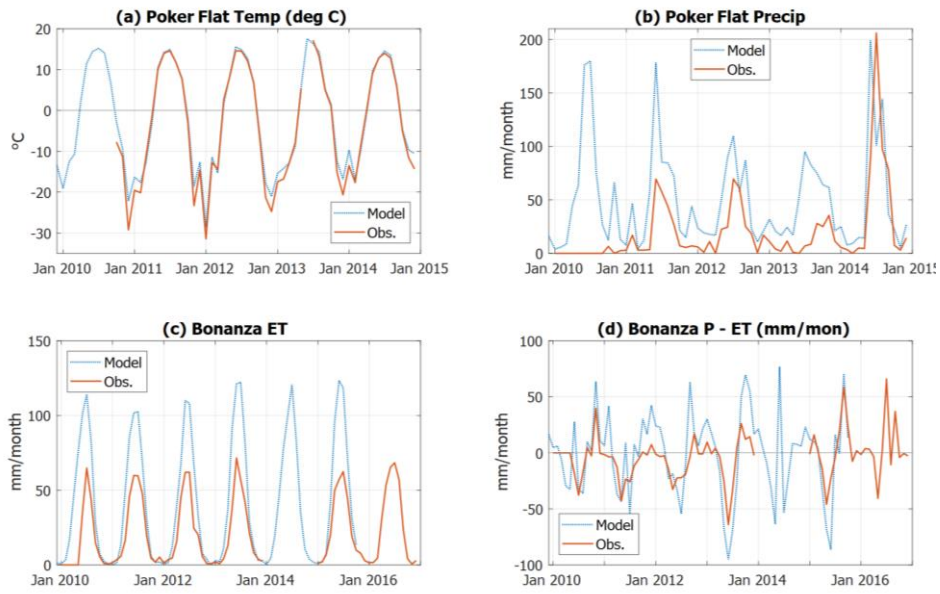


Figure 6. As in Figure 5, but for forest sites: (a) air temperature at Poker Flat, (b) precipitation, P, at Poker Flat, (c) evapotranspiration, ET, at Bonanza Creek, (d) P-ET at Bonanza Creek.

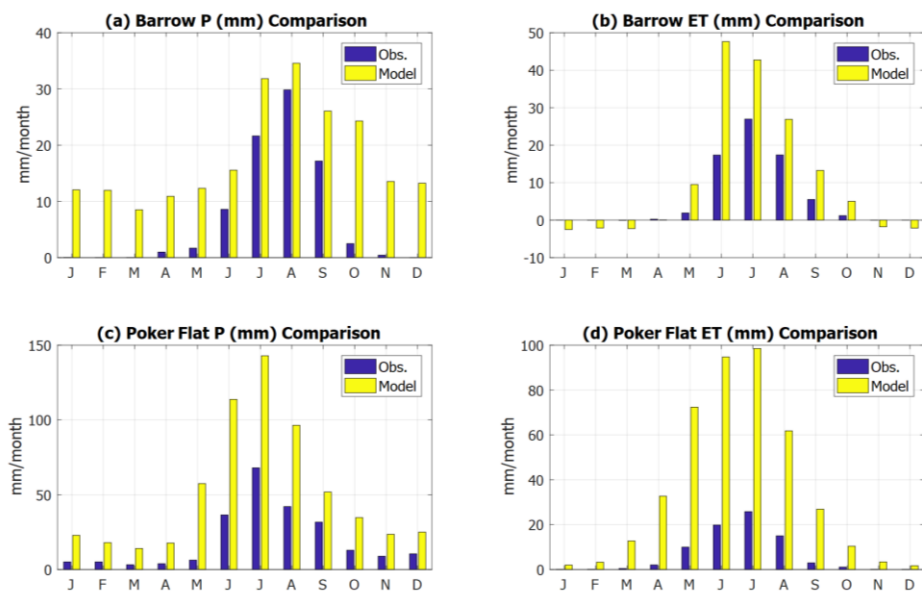


Figure 7. Monthly climatologies (averages over all available years) of tower measurements (blue) and corresponding model simulations (yellow) of (a) precipitation at Barrow, (b) evapotranspiration at Barrow, (c) precipitation at Poker Flat, and (d) evapotranspiration at Poker Flat.

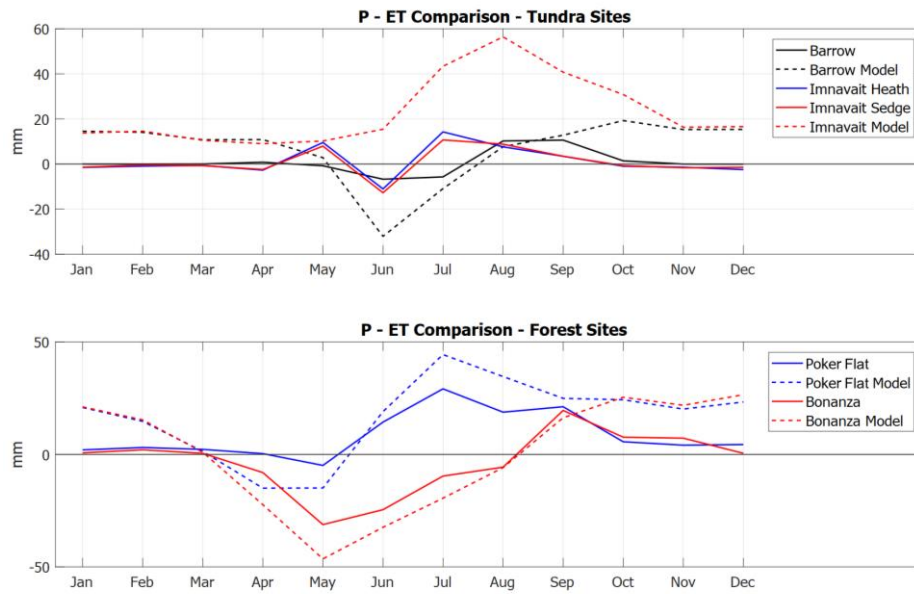


Figure 8. Climatological (average over all available years) monthly values of P-ET at tundra sites (upper panel) and forest sites (lower panel). Values derived from tower measurements are shown by solid lines, model-simulated values by dashed lines.

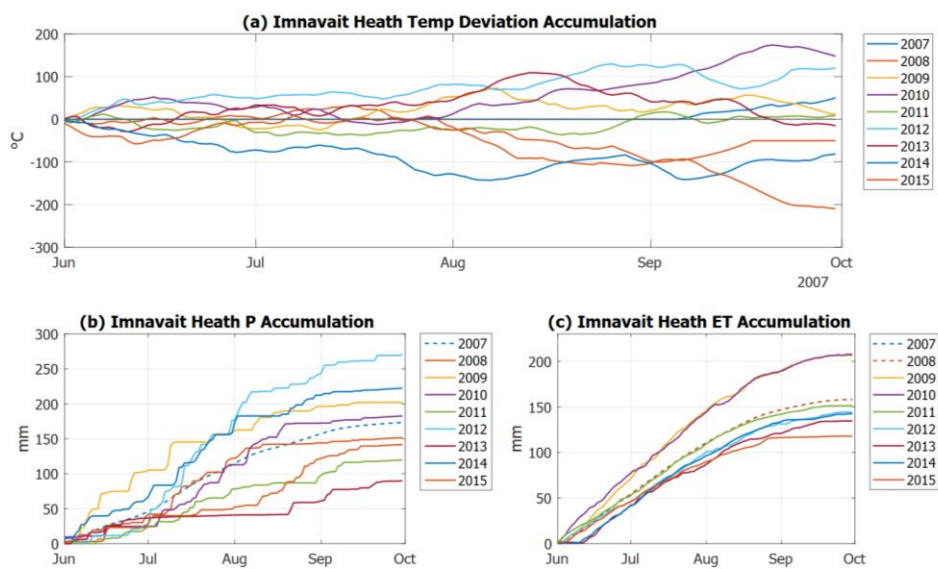


Figure 9. Seasonal (June through September) accumulations of (a) air temperature anomalies, (b) precipitation and (c) evapotranspiration at the Imnavair heath site. All values are based on tower measurements. Different years are color-coded; dashed lines are estimated values (see text) for years with large amounts of missing data.



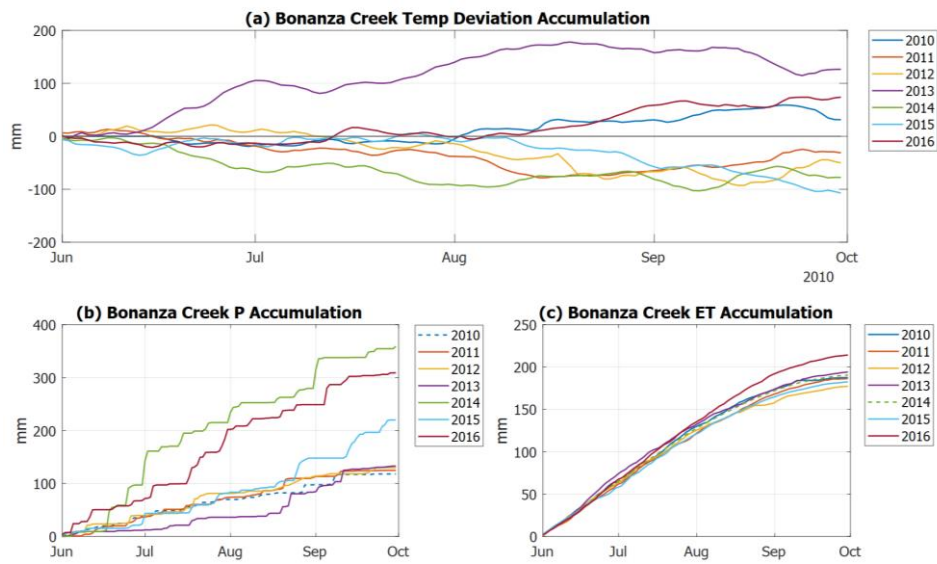


Figure 10. As in Figure 9, but for seasonal accumulations at Bonanza Creek.

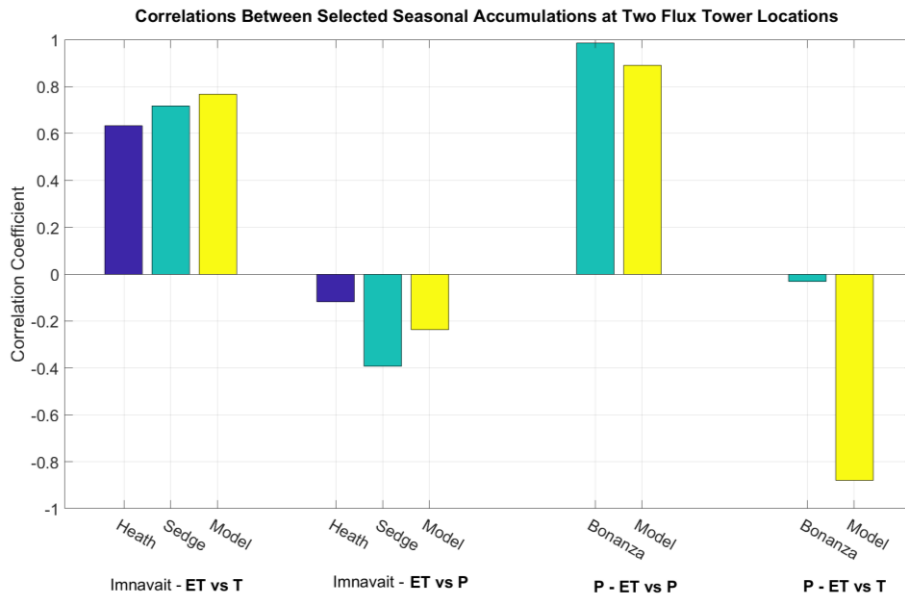


Figure 11. Sample correlations between yearly warm-season totals of ET, P-ET and driving variables (T, P). Blue and green bars are correlations based on tower data; yellow bars are correlations based on model simulation.

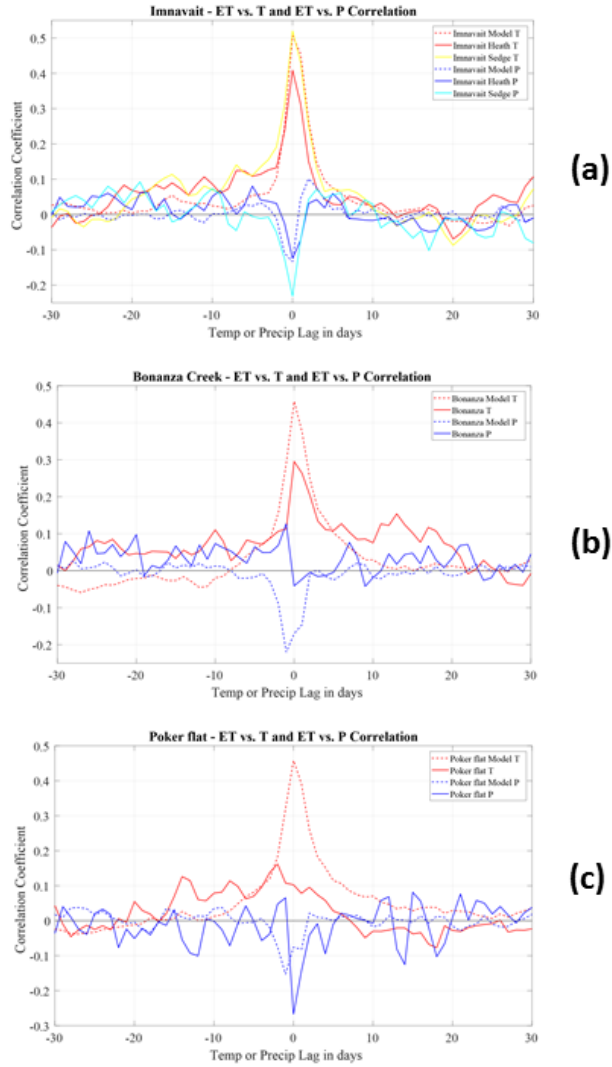


Figure 12. Cross-correlation functions of daily ET with daily temperature (red) and daily precipitation (blue) for (a) Imnavait Creek, (b) Bonanza Creek and (c) Poker Flat. Correlations are plotted as a function of the lag of P and T relative to ET (i.e., T and P lead ET to the left of zero lag; T and P lag ET to the right of zero lag). Solid lines are based on tower measurements, dashed lines on model output.

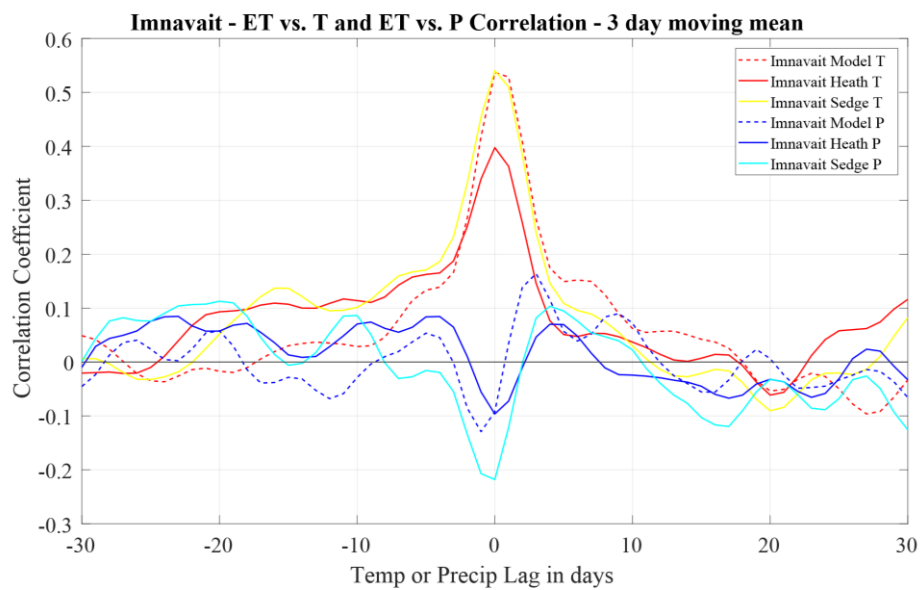


Figure 13. As in Figure 12, but for cross-correlations computed from 3-day running means of T, P, and ET at Imnavait Creek. Solid lines are based on tower measurements, dashed lines on model output. Values for wet sedge and heath are plotted in different colors.